Dimensionless Performance Model for Gas-Fed Pulsed Plasma Thrusters*

J.K. Ziemer† and E.Y. Choueiri‡
Electric Propulsion and Plasma Dynamics Laboratory (EPPDyL)
MAE Dept.
Princeton University
Princeton, New Jersey 08544

AIAA-98-3661§

Abstract

We present a non-dimensional gas-fed pulsed plasma thruster performance model. The analysis uses a circuit element discharge description and a snow-plow mass accumulation model with two non-dimensional parameters for an outer electrode geometry contour and an exponential mass distribution. Implementing a non-dimensional scheme is shown to reduce the number of free parameters in the equations from ten dimensional parameters to five non-dimensional parameters. This simplification allows the non-dimensional parameter space to be explored in terms of thrust efficiency and a defined non-dimensional thrust-to-power ratio. An electrode length providing the optimal efficiency of the discharge is determined for each configuration of non-dimensional parameters. The sensitivity of thruster performance to all five non-dimensional parameters is examined and performance scaling trends are discussed.

1 Introduction

Modeling the dynamics of a pulsed plasma thruster (PPT) discharge generally requires a complex multi-parameter model using a numerical method to generate a solution. The solution is made up of the discharge velocity, current, voltage, etc., and performance metrics such as efficiency and the thrust to power ratio can be calculated from the final state of the current sheet. To specify a particular solution, there are many parameters that must be specified *a priori* such as: the main capacitance, initial inductance, mass loading, charging voltage, plasma resistance, etc. which can preclude the usefulness of such a numerical tool for predicting optimum performance over a wide range of conditions. A correct non-dimensional scheme, however, reduces the number of free parameters to the lowest amount possible allowing a more reasonable approach for finding overall performance scaling laws.

Many simple one-dimensional models for gas-fed pulse plasma thruster (GFPPT) discharges have been published before, refs. [1, 2, 3, 4], as well as non-dimensional schemes, refs. [5, 6]. In most of these models and the model described in this paper, an inductor, capacitor, and resistor are placed in series to represent the moving discharge as an LCR circuit. The elements of this circuit are generally variable with the inductance change resulting from the current sheet motion. The circuit model coupled with a "snow-plow" mass accumulation description provide the governing equations for the current sheet.

Most of the schemes cited above also assume a planar current sheet propagating along a set of parallel electrodes with a uniform density mass distribution. The model developed by Michels, Heighway, and Johansen[6] includes a additional arbitrary mass loading function that made testing many configurations of initial mass distribution possible. The mass loading function could be set to model a propellant

*Research supported by the Air Force Office of Scientific Research, grant number: F49620-95-1-0291.

†Graduate Student, Research Assistant supported by Princeton University's Program in Plasma Science and Technology. Member AIAA.

‡Chief Scientist at EPPDyL. Assistant Professor, Applied Physics Group. Associated Faculty at the Department of Astrophysical Sciences. Senior Member AIAA.

§Presented at the 34^{th} AIAA Joint Propulsion Conference, Cleveland, OH, July 14-17, 1998.

"slug" with no mass accumulation, a uniform mass distribution, or a general polynomial distribution between the two. Although they were able to predict an optimal performance based on a non-dimensional mass loading parameter, the parameter contained both terms for both the gas loading profile and the initial charge on the capacitor. This choice of a non-dimensionalization scheme made separating the performance increase due to the initial stored energy and the mass loading difficult. In *all* previous cases, the electrode length was specified ahead of time or simply allowed to extend to infinity sometimes yielding unnecessarily confined solution sets or unrealistic solutions.

The model in this paper adds both an exponential mass distribution and a contoured outer electrode geometry to the previously published models, thus introducing two additional non-dimensional parameters. It relies on its simplicity (a modern desktop computer can numerically solve the equations in less than ten seconds) to thoroughly explore various thruster configurations. In the next section, the dimensional equations will be derived, and the non-dimensionalization process will be presented. Non-dimensional parameters will be defined and discussed as well as the solution method. The results will be presented in terms of two possible electrode lengths. One is based on the maximum efficiency that can be achieved during the discharge, and the other is based on the extent to which the current sheet travels until the capacitor has been discharged over a number of characteristic circuit time constants. These two choices of electrode length will be shown to represent opposite ends of the spectrum in terms of thruster performance. In addition, results from varying all five parameters one at a time will allow distinguishing the effect of each non-dimensional parameter on GFPPT performance. Finally, the results will be summarized into a list of suggestions for designing the next generation of high performance GFPPTs.

2 A Non-Dimensional Model for Gas-Fed Pulsed Plasma Thrusters

This section of the paper will begin by describing the physical model of the PPT discharge in more detail. First, the quasi-one dimensional approach will be presented including the outer electrode contour equation and the mass distribution equation. Next, all of the equations will be non-dimensionalized reducing the number of free parameters to obtain a unique solution from ten to only five. This small number of parameters together with the two methods for determining the electrode length allow the non-dimensional parameter space to be reasonably explored in terms of performance optimization. It will be shown that particular values of the five parameters exist that maximum thruster performance.

2.1 Quasi-One-Dimensional Equations

This quasi-one-dimensional model has an outer electrode profile, $r_{outer}(x)$, and a non-uniform mass distribution, $m(x)$. The current sheet itself is assumed to be planar and all forces are considered to act only in the axial direction. The equation describing the outer electrode contour is exponential in nature to allow a variety of geometries,

$$r_{outer}(x) = r_{out}e^{x/k}. \tag{1}$$

This equation is shown schematically in figure 1.

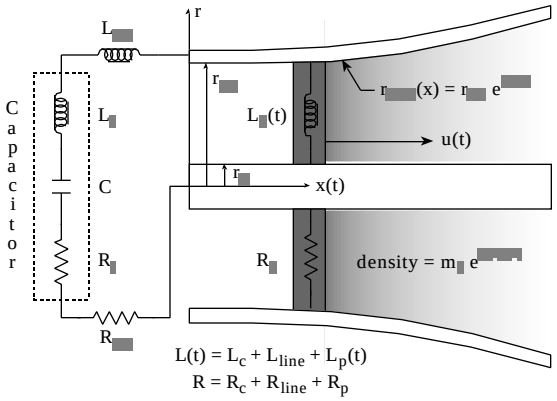

Figure 1: Schematic of quasi-one dimensional GFPPT discharge model.

The mass distribution equation used in this model is derived from a one-dimensional kinetic description of a gas column expanding into a vacuum. The gas column is originally contained by a barrier at $x = 0$ which is removed at $t = 0$. As the gas expands, the overall density profile is an error function with an exponential nature beginning at $x = 0$ some time t later. The mass distribution constant in the exponential is related to the product of the molecular speed of the gas and the expansion time. For an impermeable,

"snow-plow" current sheet, this density function can be integrated to yield the total mass, $m(x)$ collected at any point along the channel,

$$m(x) = \int_0^x m_1 e^{-x^{*2}/b^2} dx^* + m_0, \tag{2}$$

where m_1 is a density (mass per unit length), m_0 is the initial mass taken up by the current sheet initiation, and b is the mass distribution constant. Again, the exponential nature of the equation allows a uniform mass distribution for a large mass distribution constant, and a "slug" mass for a small mass distribution constant. These values can be achieved in real gas-fed thrusters by adjusting the time the propellant is allowed to flow before the discharge initiates.

As used in previous models[1, 2, 3, 4, 5, 6], the moving current sheet is modeled using Kirchhoff's Law with changing elements producing the general "circuit" equation,

$$V_0 = \frac{1}{C}\int_0^t J dt^* + \frac{d}{dt}(LJ) + RJ, \tag{3}$$

where V_0 is the initial capacitor voltage, C is the main capacitance value, J is the total current in the circuit, L is the total circuit inductance, and R is the total circuit resistance including the electronics and the plasma discharge. This circuit model is included schematically in figure 1. For the model described in this paper, the resistance will be considered constant in both space and time.

The momentum equation includes terms for current sheet acceleration, dynamic losses due to the accumulation of mass, and the electromagnetic force,

$$\frac{d}{dt}\left(m\frac{dx}{dt}\right) = \int\int\int \vec{j} \times \vec{B}\, dV_{ol}, \tag{4}$$

where $\vec{j}$ is the current density and $\vec{B}$ is the magnetic field induced by the current conducted through the discharge. This equation assumes that all the gas swept up by the current sheet is accelerated to the sheet velocity and that all the collected mass travels at one speed. It does not allow for any recovery of thermal energy into directed kinetic energy.

The inductance for this circuit increases as the current sheet expands down the electrodes. From the outer electrode profile, eqn. 1, the inductance can be calculated as a function of x for co-axial electrodes,

$$L = \frac{\mu_0}{2\pi}\left[\frac{1}{2k}x^2 + x\ln\left(\frac{r_{out}}{r_{in}}\right)\right] + L_0, \tag{5}$$

where L_0 is the initial inductance in the circuit. It is important to note that this inductance is quadratically increasing over x rather than linearly as in previous models due to the exponential nature of the outer electrode profile. At this point it is convenient to define an inductance per unit length, L_1, for a parallel co-axial set of electrodes:

$$L_1 = \frac{\mu_0}{2\pi}\ln\left(\frac{r_{out}}{r_{in}}\right). \tag{6}$$

This expression will be used in future sections to non-dimensionalize the total circuit inductance with any outer electrode contour.

Differentiating eqn. 3 with respect to time and expanding the terms yield:

$$J\left[\frac{1}{C} + \frac{dL}{dx}\frac{d^2x}{dt^2} + \frac{d^2L}{dx^2}\left(\frac{dx}{dt}\right)^2\right] + \frac{dJ}{dt}\left[R + 2\frac{dL}{dx}\frac{dx}{dt}\right] + \frac{d^2J}{dt^2}[L] = 0. \tag{7}$$

Notice that there is a second spatial derivative of the inductance that will not be zero for the case of a contoured outer electrode.

The momentum equation, eqn. 4, can also be expanded, and the integral of the Lorentz force can be evaluated over the current sheet volume to yield:

$$\frac{dm}{dx}\left(\frac{dx}{dt}\right)^2 + m\frac{d^2x}{dt^2} - \frac{\mu_0}{4\pi}J^2\left[\ln\left(\frac{r_{out}}{r_{in}}\right) + \frac{x}{k}\right] = 0. \tag{8}$$

To solve these equations a total of ten parameters ($r_{out}, r_{in}, k, m_0, m_1, b, V_0, C, R, and\ L_0$) must be specified along with an integration period or propagation distance (electrode length) to generate a unique solution. Clearly with this many parameters and a choice of discharge length, it would be difficult to determine an optimal thruster design or discover any trends in performance related to a particular dimensional parameter. In the next section, however, a non-dimensionalization scheme will reduce the number of parameters in half allowing the non-dimensional parameter space to be spanned for exploring performance optimization.

2.2 Non-Dimensional Variables and Parameters

Except for a few special cases, analytical solutions to eqns. 7 and 8 are not available. However, one of these special analytical solutions provides the non-dimensionalization scheme used here. In a critically

damped LCR circuit with constant circuit elements, the maximum current is reached at $t = \sqrt{L_0 C}$ with a value, $J_{peak} \approx 1/3\ V_0\sqrt{C/L_0}$. For the movable current sheet, we are concerned with the characteristic length it will take to double the initial inductance. With this in mind, we can now define the primary non-dimensional variables for time, current, and length as follows:

$$\tau = \frac{t}{\sqrt{L_0 C}}, \tag{9}$$

$$\zeta = \frac{3}{V_0}\sqrt{\frac{C}{L_0}}J, \tag{10}$$

$$\delta = \frac{L_1}{L_0}x, \tag{11}$$

In order to non-dimensionalize the full equation set, five non-dimensional parameters are required:

$$\alpha = \frac{L_1^3 V_0^2 C^2}{18 L_0^2 m_1}, \tag{12}$$

$$\psi = \frac{R}{2}\sqrt{\frac{C}{L_0}}, \tag{13}$$

$$\rho_0 = \frac{m_0 L_1}{m_1 L_0}, \tag{14}$$

$$\gamma = \frac{L_0}{L_1 b}, \tag{15}$$

$$\lambda = \frac{\mu_0}{2\pi}\frac{L_0}{L_1^2}\frac{1}{k}. \tag{16}$$

The first three parameters have been defined in a similar fashion in previous works, refs. [5]. The last two are introduced here and determine the exponential nature of the mass distribution and the flare of the outer electrode, respectively. All of these parameters will be discussed in more detail in section 2.5.

Using these definitions, the mass accumulation can also be expressed as a non-dimensional variable, ρ:

$$\rho = m\frac{L_1}{m_1 L_0} = \int_0^\delta e^{(-\gamma^2\delta^{*2})}d\delta^* + \rho_0. \tag{17}$$

The inductance is now a function of δ and λ,

$$L = L_0\left(\frac{1}{2}\lambda\delta^2 + \delta + 1\right). \tag{18}$$

With all the primary variables and parameters defined, we can express the two main equations for energy and mass conservation non-dimensionally.

2.3 The Circuit Energy Equation

The circuit equation, eqn. 7 becomes:

$$\zeta\left[1 + \lambda\left(\frac{d\delta}{d\tau}\right)^2 + (1+\lambda\delta)\left(\frac{d^2\delta}{d\tau^2}\right)\right] + 2\frac{d\zeta}{d\tau}\left[\psi + (1+\lambda\delta)\frac{d\delta}{d\tau}\right] + \frac{d^2\zeta}{d\tau^2}\left[\frac{1}{2}\lambda\delta^2 + \delta + 1\right] = 0. \tag{19}$$

There are many terms in this equation related to the curvature of the outer electrode that are not present in previous models. As the quantity $\lambda\delta$ approaches unity, these terms dominate over the normal parallel electrode configuration.

2.4 Mass Addition and Momentum Conservation

Under this non-dimensionalization scheme, the momentum equation becomes:

$$\frac{d\rho}{d\delta}\left(\frac{d\delta}{d\tau}\right)^2 + \rho\frac{d^2\delta}{d\tau^2} - \alpha(1+\lambda\delta)\zeta^2 = 0. \tag{20}$$

Again, there are terms here that are present due to the contoured nature of the outer electrodes and the exponential mass distribution function. Overall this equation shows that the current sheet acceleration, $d^2\delta/d\tau^2$ is due to the driving electromagnetic force, $\alpha(1+\lambda\delta)\zeta^2$, minus the momentum change required to bring the mass just in front of the current sheet up to speed, $d\rho/d\delta(d\delta/d\tau)^2$. This momentum is lost to internal thermal energy and is not recovered.

2.5 Summary of Non-Dimensional Parameters

This section of the paper will go into more detail regarding the five non-dimensional parameters now classified as: The dynamic impedance parameter α, the critical resistance ratio ψ, the initial mass parameter ρ_0, the mass distribution parameter γ, and the geometry parameter λ.

2.5.1 The Dynamic Impedance Parameter, α

The dynamic impedance parameter is the most complicated of the non-dimensional parameters. It is a combination of ratios that include: the change in inductance to the initial inductance, $\Delta L/L_0$, typically a measure of PPT efficiency with a value greater than

unity; the dynamic impedance to the circuit resistance ratio, $\dot{L}_f/R$, again, this ratio should be greater than one for PPTs that are electromagnetic in nature; the inverse of the thrust efficiency, $1/\eta$, which will be greater than one; and the critical resistance ratio which is typically of order one or less. Together with the 2/9 coefficient, α should be close to unity for most GFPPTs. This expansion of α in terms of ratios is presented below along with another interpretation of the dynamic impedance parameter,

$$\alpha = \frac{2}{9}\frac{\Delta L}{L_0}\left(\frac{\dot{L}_f}{R}\right)^2 \frac{1}{\eta}\,\psi^2, \tag{21}$$

$$= \frac{8}{9}\frac{L_1^3 V_0^2}{R^4 m_1}\psi^4. \tag{22}$$

The second relation shows that α is proportional to the resistance parameter ψ to the fourth power. This formulation presents α without any direct dependence on the capacitance or initial inductance. In the results section4.2, this formulation will prove to be useful in describing thruster performance scaling.

2.5.2 The Critical Resistance Ratio, ψ

This ratio describes the oscillatory nature of the current waveform. Together with the changing inductance, $\dot{L}$, this parameter determines if the circuit response is over, under, or critically damped. This parameter will be shown to be the most important in determining thruster performance. Typical values are of order unity or slightly smaller.

2.5.3 The Initial Mass Parameter, ρ_0

The initial mass parameter is simply a ratio of the initial mass in the current sheet formation to the total mass accumulated after traveling to $\delta = 1$ with a uniform mass distribution. For most gas-fed PPTs, this parameter is small, close to 0.5 or less.

2.5.4 The Mass Distribution Parameter, γ

This parameter describes the distribution of mass in the thruster. As seen from eqn. 17, large values of γ lead to mass distributions concentrated near the breech of the electrodes. As γ approaches zero, the mass is distributed uniformly with a linear density of m_1.

2.5.5 The Geometry Parameter, λ

This parameter describes the contour of the outer electrode. Large values of λ lead to severely expanded outer electrodes that in some extreme cases can be considered unrealistic. In addition, large values of λ can bring the quasi-one-dimensional assumption of the planar current sheet into question. Values of λ close to 0.1 provide a slight flare that should be enough to indicate the benefits of using an expanding outer electrode. Notice that if λ is set to zero, the electrode set becomes parallel, and the circuit and momentum equations (eqns. 19 and 20) used in previous work are recovered.

2.6 Performance Benchmarks: Efficiency and Thrust to Power Ratio

Before discussing the model solution methodology and results, it is important to define our objectives. The performance of a PPT is defined by two quantities: thrust efficiency and the thrust to power ratio. Efficiency is defined in the usual sense, a ratio of the directed kinetic energy to the energy stored initially in the capacitor:

$$\eta = \frac{\frac{1}{2}m_{bit}u_e^2}{\frac{1}{2}CV_0^2} = \frac{1}{18}\frac{\rho\dot{\zeta}^2}{\alpha}, \tag{23}$$

where we have also expressed η in terms of the model's non-dimensional parameters.

Similarly, the thrust to power ratio can be expressed as a function of the model's non-dimensional parameters,

$$\frac{T}{P} = \frac{I}{E} = \frac{m_{bit}u_e}{\frac{1}{2}CV_0^2} = \frac{1}{9}\frac{\rho\dot{\zeta}}{\alpha}L_1\sqrt{\frac{C}{L_0}}, \tag{24}$$

however, since T/P is a dimensional quantity, some dimensional parameters are required in its definition. We now set a new metric called the "non-dimensional thrust to power ratio" without the particular circuit parameters of L_0, L_1, *and* C,

$$\left(\frac{T}{P}\right)^* = \frac{1}{9}\frac{\rho\dot{\zeta}}{\alpha}. \tag{25}$$

Although there can be other definitions for this performance indicator in terms of additional non-dimensional parameters (for example replacing $\sqrt{C/L_0}$ with $2\psi/R$,) this definition will be used for its simplicity and the lack of ambiguity in evaluating the initial inductance, inductance per unit length, and capacitance required to change this parameter into an actual value for a given thruster.

Performance optimization is often a trade-off between high efficiency and a large thrust to power ratio. In general, a thruster should be configured to satisfy the requirements of a specific mission. However, without a particular mission in mind, we will explore the sensitivity of both η and $(T/P)^*$ to the relevant non-dimensional parameters of the model.

3 Numerical Solution of Non-Dimensional Equations with Varying Parameters

After specifying the five non-dimensional parameters, eqns. 19 and 20 can be solved numerically to produce non-dimensional current, position, velocity, and mass waveforms related to the current sheet propagation. The equations can be integrated over an arbitrary number of characteristic time constants ($\sqrt{L_0 C}$) until the capacitor is discharged or another termination condition has been imposed. From the output waveforms, the thrust efficiency and the non-dimensional thrust to power ratio can be calculated at any time during the discharge. This section of the paper will discuss the numerical integration scheme, verification of the model, imposed termination conditions, and spanning of the non-dimensional parameter space.

3.1 Two-time Step Integration Scheme

To solve the final non-dimensional equations, a numerical integration scheme was employed requiring the choice of an integration time step. In order to reduce the error in solving the equations, two time step sizes were used during different parts of the integration as shown in figure 2. For most discharges, the derivatives of the position and current change the most drastically during the first few characteristic time constants. For this first period of integration, a small time step is required (typically $\sqrt{L_0 C} \times 10^{-}5$) to have a constant solution independent of small changes in the time step size. Later in the discharge, during the exponential decay of the current for example, the primary variables change much more slowly. Although the discharge may remain dynamic for many characteristic time lengths, to keep computational time down the integration time step may be reduced by a factor of 10 or more. Between the two regions, a linear interpolation of the primary variables and their derivatives is performed to maintain a smooth transition.

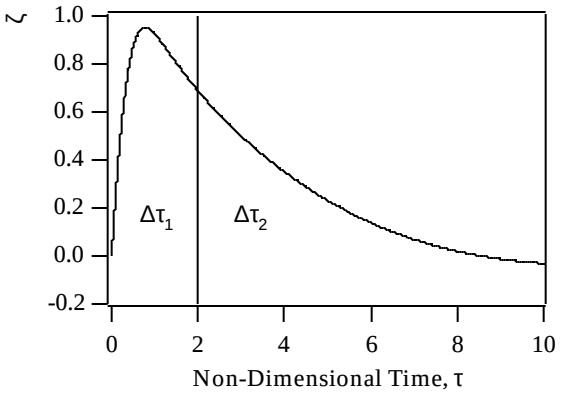

Figure 2: Integration scheme with two time step sizes.

3.2 Verification of the Model

The model was verified computationally in two ways: 1) by comparing results from fixed circuit parameters to available analytical solutions, and 2) by numerically calculating the derivatives from the integrated position and current variables and insuring that eqns. 19 and 20 are true. The second method was used each time the program was run to insure that a small enough time step was used. For all the results presented here, the largest absolute difference between the computational results and the expected output was 0.5%. Decreasing the time step size did not change the error by a significant amount, however, increasing the time step by a factor of 100 increased the error by a factor of 10. The criteria for an acceptable solution was a maximum error in the calculated derivatives of less than 1%.

3.3 Termination Conditions

The numerical integration of the circuit and mass addition equations requires a specified final time to end the calculation. Theoretically, this occurs when the capacitor is fully discharged, however, for some parameter configurations, this can be a very long time. For discharges that last longer then ten $\sqrt{L_0 C}$ time constants, the requirement to fully drain the capacitor results in very long and unrealistic electrode geometries. In addition, with mass accumulation being specified as a function of x, long integration times can result in heavily loaded-down current sheets traveling very slowly. Although the thrust typically continues to build, the product of the mass and velocity squared, and therefore the efficiency, decreases.

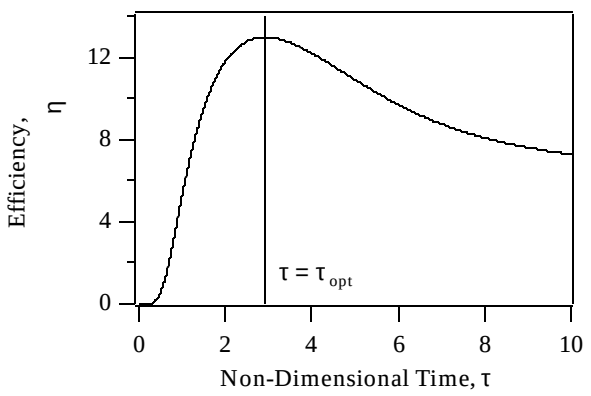

Figure 3: τ_{opt} is set when efficiency reaches its maximum value during the discharge.

Therefore, choice of the integration duration is important in evaluating thruster performance. For this model, this period was specified in two ways: 1) by determining the optimal period for maximum efficiency, and 2) using a limited number of characteristic time constants to prevent solutions that require extreme electrode length and mass bit values while insuring that most of the capacitor energy has been drained.

3.3.1 Optimal Efficiency Electrode Length

For almost every non-dimensional parameter configuration, there exists an integration duration that maximizes efficiency. This period will be defined as τ_{opt} and is shown in figure 3. The optimum electrode length definition follows,

$$(l_{electrode})_{\eta opt} = \delta(\tau_{opt}). \tag{26}$$

Except for the cases when the exponential nature of the mass distribution reduces the mass accumulation at large δ (typically this occurs for $\gamma > 0.2$), the efficiency will have a maximum occurring *before* the full extent of the capacitor discharge. This means that after this point the current sheet is slowing down due to the accumulation of mass even though there is still charge left on the capacitor. At this τ_{opt}, it becomes more profitable in terms of directed kinetic energy to terminate the length of the electrodes, and, therefore, mass accumulation as well as energy addition. Although at this point there is still energy in the capacitor, in terms of overall efficiency, it becomes more beneficial to let this energy be: a) recovered by some switching technology between the capacitors and the electrodes, or b) even lost to a highly resistive "crowbar" discharge at the breech of the thruster. This conclusion is based on the lack of thermal energy recovery in the momentum equation which has been shown to be a good assumption for many low density plasma flows[7, 8]. Although it may seem counterproductive to waist the remaining energy rather than try to recover it, from an efficiency stand point, it is not advantageous to do so.

3.3.2 Fixed Integration Time

The other end of the performance spectrum is to let the discharge propagate down the electrodes accumulating mass until there is no charge left on the capacitors. For that case, the product of the mass and velocity, $\rho\dot{\delta}$, will continue to increase and eventually reach an asymptote. That is to say that the thrust will continue to increase even as the the total mass accumulated by the discharge rises and the current sheet slows down. As mentioned before, care must be taken to choose a limit of integration to preclude solutions which generate long electrode geometry requirements. With this in mind, the integration will be stopped at $\tau = 10$. Although in some cases presented here a minimal amount of charge will be left in the capacitor, usually this is less than 5% of the total stored energy, and extending the discharge further will not change the results significantly. For parameter sets where there is a larger fraction of stored energy on the capacitor, the solution is discarded and the parameter is not varied past that value as discussed in the next section.

3.4 Spanning the Parameter Space

After the limits of numerical integration are set, the computational model can be used successively with different values of the non-dimensional parameters. After each trial, new values of performance are calculated and recorded. With typical computational times of four seconds per trial on a desktop computer, it was easy to span a significant parameter space thoroughly enough to determine meaningful trends. In addition, limits were set on the range of parameter variation depending on the typical values for the parameter in real thruster designs, and on whether such a thruster configuration is realistic.

First, it was determined from recent gas-fed pulsed plasma thrusters[4] that values of the non-dimensional parameters are close to $\alpha = 1$, $\psi = 0.5$, $\rho_0 = 0.5$, $\lambda \approx 0.1$, and $\gamma \approx 0.1$. In most cases,

the variation of each parameter was an order of magnitude on either side of this typical value. For ρ_0, γ, and λ, however, stretching into higher values created unrealistic electrode lengths with $\Delta L/L_0 > 100$.

4 Results

A complete set of results is shown at the end of this paper including sixteen graphs of thruster performance with various parameters altered. There are two types of data presentation, one where only one parameter was varied, and the other where two parameters where varied producing performance level curves. These results will be discussed on a parameter basis in the following section.

4.1 Variation of One Parameter

In each case, one parameter at a time was varied while the rest of the parameters remained at constant values for a typical GFPPT: $\alpha = 1$, $\psi = 0.5$, and $\rho_0 = 0.5$. The effect of the outer electrode contour as well as the exponential mass distribution is also shown by slightly changing λ or γ for each case. These three curves ($[\gamma = 0, \lambda = 0], [\gamma = 0, \lambda = 0.2]$, and $[\gamma = 0.2, \lambda = 0]$) are shown for both the optimal electrode length (in bold, thicker lines) and the full extent of the integration period in figures 4 and 5. Figure 4 shows the thruster efficiency for each varying parameter, and figure 5 shows the non-dimensional thrust to power ratio for each varying parameter. Each of the parameters will now be discussed in detail.

4.1.1 Variation of the Dynamic Impedance Parameter, α

In general, α is a measure of how fast the inductance changes in the discharge. Large values lead to high sheet velocities and electrode lengths. Figure 4 (a) shows that efficiency increases as α increases as well as the benefit of using the optimum electrode length. In addition, both the flared outer electrode and the exponential mass distribution had a slightly beneficial effect on efficiency with increasing α. For $\alpha > 2$, the optimal electrode length stretched out to the full extent of the integration period for the exponential mass distribution, $\gamma = 0.2$. These solutions, however, tended to require an electrode set with a change in inductance 20 or more times greater than the initial inductance which could be hard to achieve for co-axial geometries. The non-dimensional thrust to power ratio in figure 5 (a) is shown to decrease with increasing alpha. This is a result of the inductance per unit length increasing while the propellant density is decreasing creating high exhaust velocities with little mass or thrust. In this case, flaring the outer electrode improved the thrust to power ratio slightly, however, increasing the exponential nature of the mass distribution had almost no effect.

Therefore, it appears that depending on the mission requirements for the thruster application, high efficiency or high thrust to power ratio, α should be chosen accordingly.

4.1.2 Variation of the Critical Resistance Ratio, ψ

In both the efficiency and the non-dimensional thrust to power ratio, it is clear from figures 4 and 5 (b) that ψ should be reduced to as low a value as possible. For efficiency concerns, here again it is important to use the optimal electrode length unless the propellant distribution is exponential ($\gamma > 0.2$). In addition, flaring the electrodes seems to increase both the efficiency and the thrust to power ratio slightly; however, the exponential mass distribution actually lowers the thrust to power ratio for small values of ψ when the discharge is allowed to run to the full extent of the electrodes.

4.1.3 Variation of the Initial Mass Parameter, ρ_0

Figures 4 and 5 (c) show that the initial mass parameter does not play much of a role in GFPPT performance unless it reaches values above unity. For the case of optimal efficiency electrode lengths, a value of ρ_0 near 2 seems to be the best choice. Designing an actual mass feeding system that leads to values of ρ_0 greater than unity, however, can be difficult for GFPPTs.

4.1.4 Variation of the Mass Distribution Parameter, γ

Varying γ has more effect on efficiency than on the thrust to power ratio. This may largely be understood from a dynamic efficiency stand-point as sweeping up less mass late in the discharge reduces the thermal losses associated with bringing the mass in front of the current sheet up to speed[7]. Here again, it is more straight-forward to see that values of γ greater than two lead to the optimal efficiency electrode length being the same as the full extent of the electrodes. In addition, the combination of flaring the

outer electrode and having an exponential mass distribution seems to be beneficial for both the efficiency and the non-dimensional thrust to power ratio.

4.1.5 Variation of the Electrode Geometry Parameter, λ

Having an outer electrode that exponentially expands tends to increase both the efficiency and the thrust to power ratio. This is due to the non-linear nature of the inductance profile and not thermal recovery of kinetic energy due to expansion. Clearly larger values of λ are better, however, again we come against the notion of realistic electrode shapes and sizes as well as the validity of this model in predicting the performance of more extreme two-dimensional geometries. It should also be mentioned that *negative* values of λ (electrodes having a contracting geometry) decreased both the efficiency and the non-dimensional thrust to power ratio when compared to parallel geometry performance.

4.2 Variation of Two Parameters

Graphs 6 and 7 show how efficiency, thrust to power, and the required inductance change (effectively electrode length) change with α, ψ, and γ. For these cases, λ is zero (parallel electrodes) and γ is varied between a linear mass distribution, $\gamma = 0$, and an exponential distribution, $\gamma = 0.2$. In all cases, the optimal electrode length has been used to terminate the calculation. Although not shown here, increasing λ and rho_0 did slightly change the thruster performance, however, their effect was only slight compared to the effect of α, ψ, and γ.

Graphs 6 (a) and (b) can be broken up into two characteristic regions, below and above $\psi = 0.2$. In the region below $\psi = 0.2$, a maximum efficiency exists near $\alpha = 1$. At ψ values greater than 0.2, the efficiency levels follow more of a straight line on the logarithmic scale indicating a power relation. Going back to eqn. 22, we see that α is proportional to ψ to the fourth power and the coefficient $\frac{8}{9}\frac{L_1^3 V_0^2}{R^4 m_1}$. Staying on these parallel contours becomes as simple as changing the value of this coefficient. Therefore, higher values of the inductance per unit length, the initial voltage (energy) of the capacitor, or lower values of the circuit resistance and mass per unit length lead to higher efficiencies without changing the capacitance, initial inductance, or any other parameter. This fact especially points to higher efficiencies obtainable at higher discharge energies and lower resistance values without changing other thruster parameters. In graph 6 (b), the region below $\psi = 0.2$ shows that $(T/P)^*$ decreases proportionally to decreases in α and remains almost independent of ψ. In the region above $\psi = 0.2$, $(T/P)^*$ is constant over the variation in α and decreases with increasing ψ. Graph 6 (c) shows that the optimal electrode length is a strong function of α and not ψ.

For all of the data presented in figure 7, the optimal efficiency electrode length is actually the electrode length at the end of the integration period, $10\sqrt{L_0 C}$. As seen in graphs 7 (a) and (c) of that figure, the optimal value of $\alpha \approx 1$ in the previous linear mass distribution case is no longer true. Large values of α lead to very high efficiencies, however, they also require very large changes in inductance and unrealistic requirements for electrode geometry. Graph 7 (b) shows that the functional dependency of $(T/P)^*$ on α and ψ does not change much from increasing γ, however, the magnitude has increased slightly.

At this point it should be noted that the theory outlined in this paper has not been compared to the GFPPT performance data bases in refs. [4] and [9]. The impulse data taken with small mass bit values in those papers is currently under investigation for contamination due to diffusion pump oil and should not be considered a valid indication of GFPPT performance. A new GFPPT database with the contamination problem resolved will be presented as soon as possible.

5 Summary and Comments

The simplicity of the non-dimensional approach used in this paper has allowed meaningful trends in gas-fed pulsed plasma thruster performance to be explored through the variation of a small number of non-dimensional parameters. Included in these non-dimensional parameters are two new parameters that define the exponential nature of the outer electrode contour and the initial mass distribution. This model has used an optimal efficiency electrode length to compare the performance between various non-dimensional parameter values. The following conclusions regarding the two new parameters have been presented:

- Using a flared outer electrode slightly increases both the efficiency and the non-dimensional thrust to power ratio.
- Using an initial exponential mass distribution is beneficial in terms of increasing efficiency with-

out noticeably effecting the thrust to power ratio; however, unrealistically large electrode geometries can be required in some extreme cases.

In terms of the other three non-dimensional parameters, the most important conclusions are summarized here:

- Small values of ψ have the highest values of efficiency and the non-dimensional thrust to power ratio.
- For values of $\psi < 0.2$, there exists an optimum in efficiency near $\alpha = 1$.
- In general, increasing α increases the efficiency and decreases the non-dimensional thrust to power ratio; however, unrealistically large electrode geometries can be required for larger values of α.
- Both efficiency and the non-dimensional thrust to power ratio are not strong functions of ρ_0 over typical values for GFPPTs.

The scaling trends reported here provide a framework for further experimental study and parametric design of gas-fed pulsed plasma thrusters.

References

[1] L.C. Burkhardt and R.H. Lovberg. Current sheet in a coaxial plasma gun. *The Physics of Fluids*, 5(3):341–347, March 1962.

[2] P.J. Hart. Plasma acceleration with coaxial electrodes. *The Physics of Fluids*, 5(1):38–47, January 1962.

[3] D. Keefer and R. Rhodes. Electromagnetic acceleration in pulsed plasma thrusters. In 25^{th} *International Electric Propulsion Conference*, Cleveland, Ohio, August 24-28 1997. IEPC 97-035.

[4] J.K. Ziemer, E.Y. Choueiri, and D. Birx. Trends in performance improvements of a gas-fed pulsed plasma thruster. In 25^{th} *International Electric Propulsion Conference*, Cleveland, Ohio, August 24-28 1997. IEPC 97-040.

[5] R.G. Jahn. *Physics of Electric Propulsion*. McGraw-Hill, 1969.

[6] C.J. Michels, J.E. Heighway, and A.E. Johansen. Analytical and experimental performance of capacitor powered coaxial plasma guns. *AIAA Journal*, 4(5):823–830, May 1966.

[7] N.A. Black and R.G. Jahn. Dynamic efficiency of pulsed plasma accelerators. *AIAA Journal*, 3(6):1209–1210, June 1965.

[8] D.E.T.F. Ashby. Energy loss in pulsed coaxial plasma guns. *AIAA Journal*, 3(6):1045–1047, June 1965.

[9] J.K. Ziemer, E.A. Cubbin, E.Y. Choueiri, and D. Birx. Performance characterization of a high efficiency gas-fed pulsed plasma thruster. In 33^{rd} *Joint Propulsion Conference*, Seattle, Washington, July 6-9 1997. AIAA 97-2925.

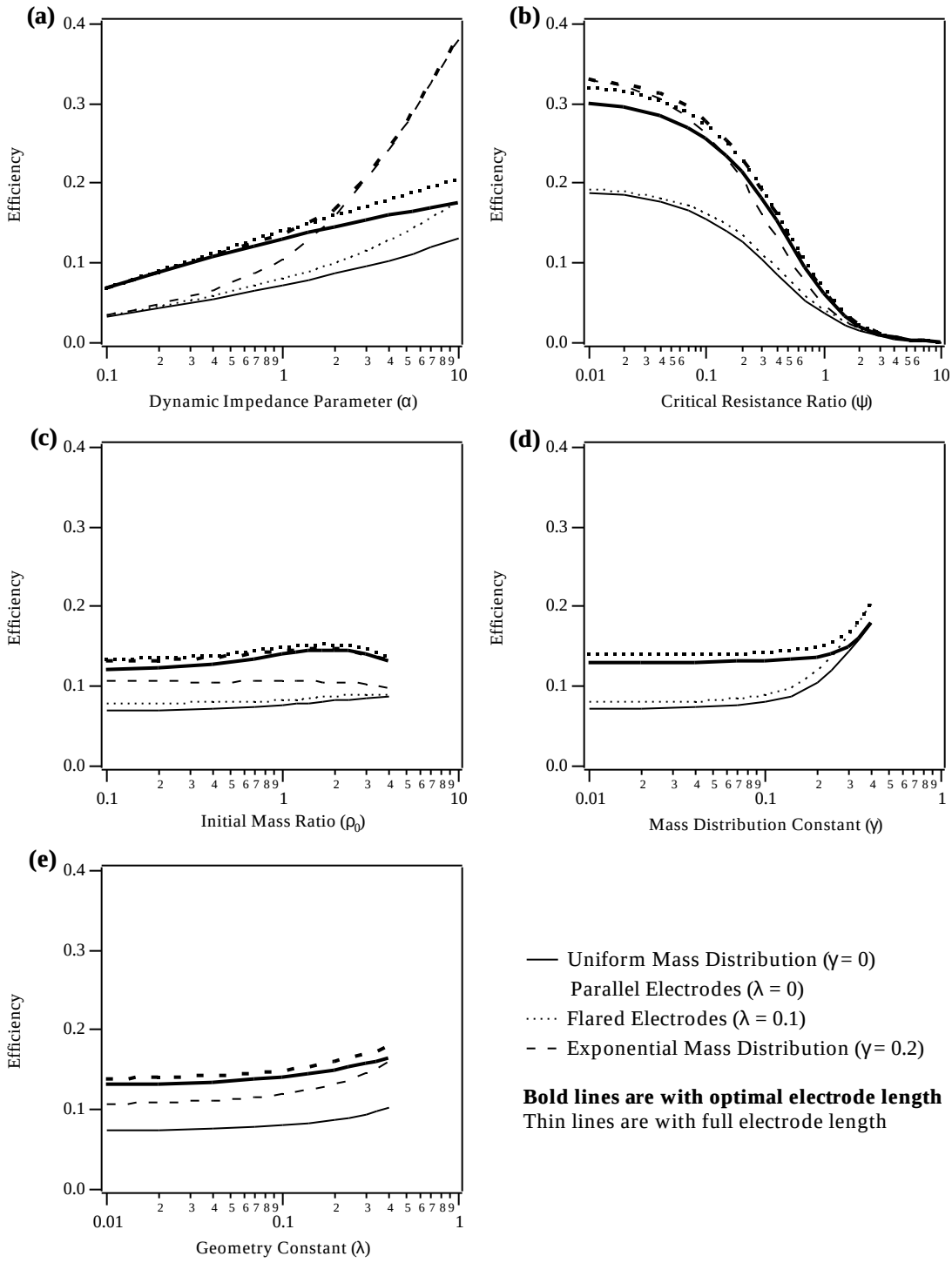

Figure 4: Graphs of the efficiency for varying (a) α, (b) ψ, (c) ρ_0, (d) γ, and (e) λ. Each graph shows three sets of curves for varying the electrode geometry and mass distribution, and two sets of curves for different electrode length choices. When one parameter is varied, others are held constant at: $\alpha = 1$, $\psi = 0.5$, and $\rho_0 = 0.5$.

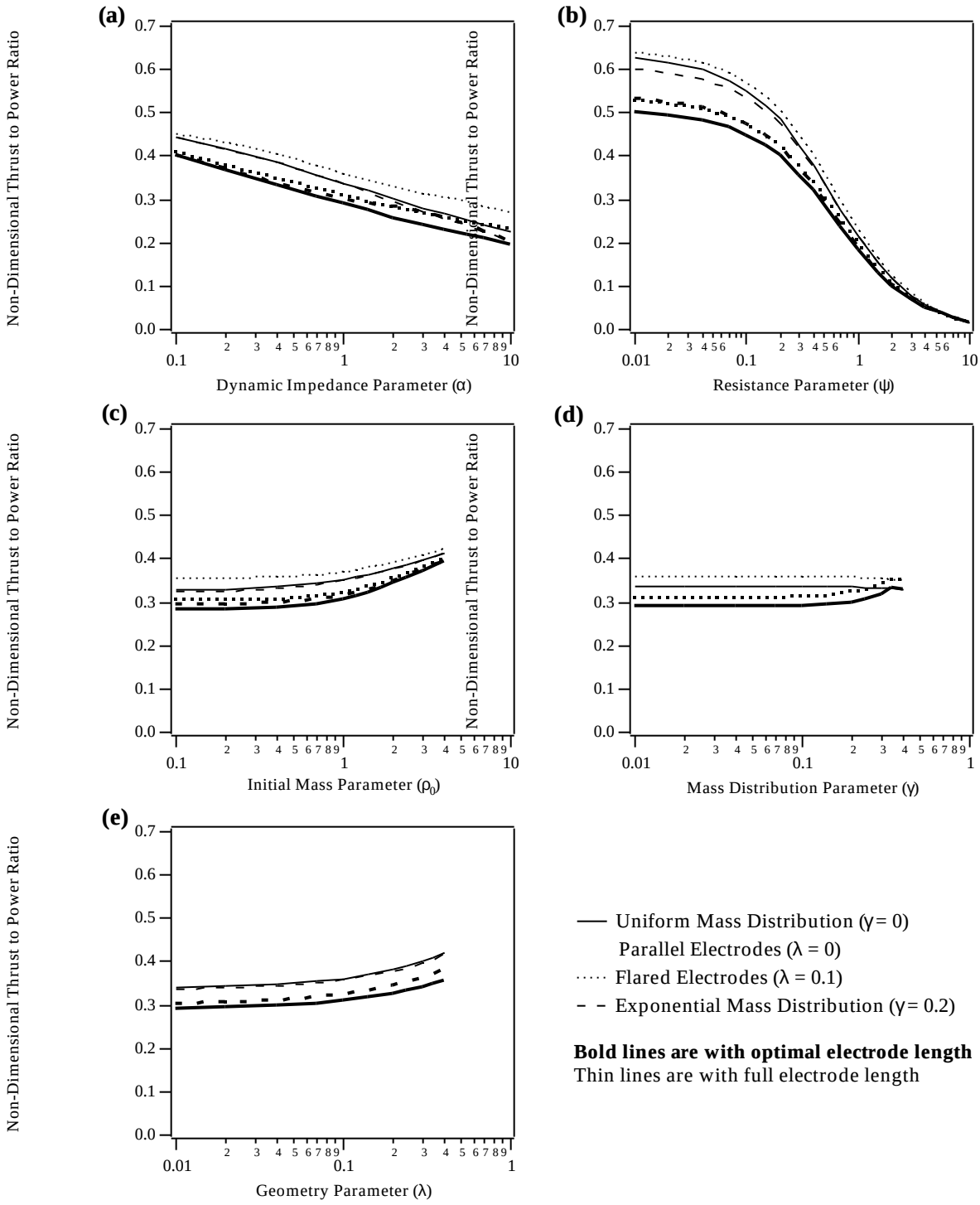

Figure 5: Graphs of the non-dimensional thrust to power ratio for (a) α, (b) ψ, (c) ρ_0, (d) γ, and (e) λ. Each graph shows three sets of curves for varying the electrode geometry and mass distribution, and two sets of curves for different electrode length choices. When one parameter is varied, others are held constant at: $\alpha = 1$, $\psi = 0.5$, and $\rho_0 = 0.5$.

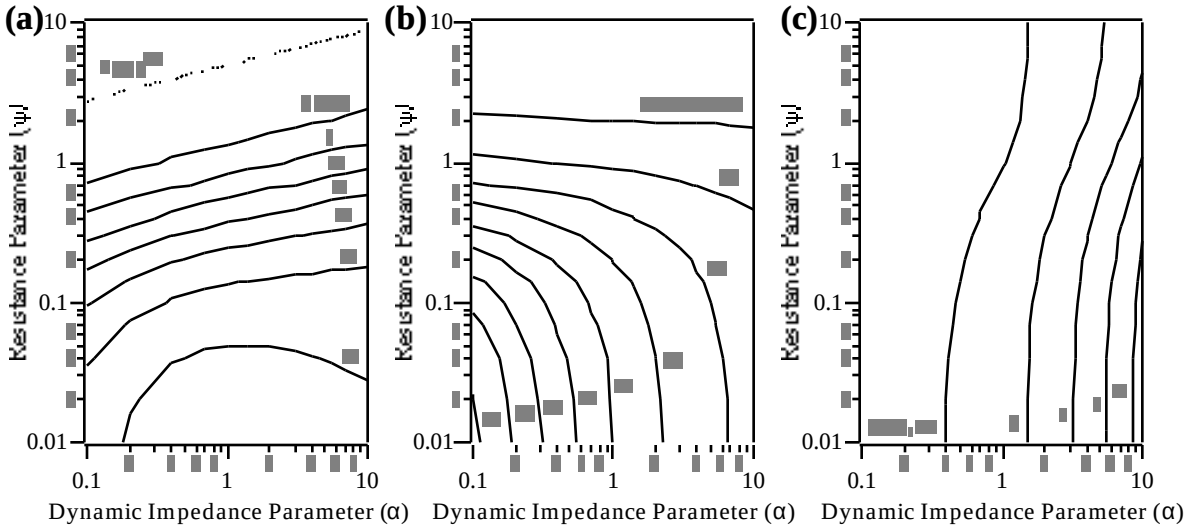

Figure 6: Contours of (a) optimum efficiency, (b) non-dimensional thrust to power ratio, and (c) required inductance change (electrode length) for $\gamma = 0,\ \lambda = 0$. The relation between α and ψ (eqn. 22) is also shown on graph (a) to match with the slope of the upper contours.

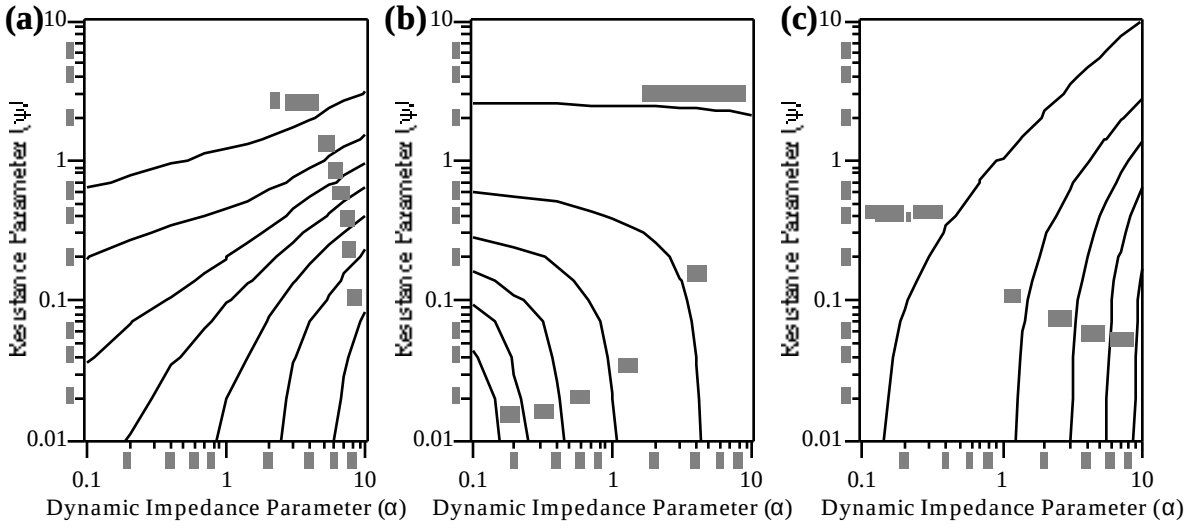

Figure 7: Contours of (a) optimum efficiency, (b) non-dimensional thrust to power ratio, and (c) required inductance change (electrode length) for $\gamma = 0.2,\ \lambda = 0$. For many of the contours, the optimal efficiency occurs at the full length of the electrode set.